J Solid State Electrochem (2009) 13:455–467
DOI 10.1007/s10008-008-0581-8

ORIGINAL PAPER

Optimization on fabrication and performance of A-site-deficient $La_{0.58}Sr_{0.4}Co_{0.2}Fe_{0.8}O_{3-\delta}$ cathode for SOFC

Fu Qiang · KeNing Sun · NaiQing Zhang · ShiRu Le · XiaoDong Zhu · JinHuo Piao

Received: 14 February 2008 / Accepted: 4 May 2008 / Published online: 4 June 2008

Abstract A-site-deficient perovskite cathode material $La_{0.58}Sr_{0.4}Co_{0.2}Fe_{0.8}O_{3-\delta}$ (L58SCF) is coated on the yttria-stabilized zirconia electrolyte by screen-printing technique. Several key fabrication parameters including selection of additives (binder and pore former), effect of coating thickness, sintering temperature and time on the microstructure, and electrochemical performance of cathode are investigated by scanning electron microscopy and electrochemical impedance spectroscopy. We study the microstructure and the electrochemical property of the cathode with different kinds of additives. Results show that the cathode possesses fine microstructure, enough porosity, and ideal electrochemical property when polyvinyl butyral serves as both binder and pore former in the cathode. The cathode with three screen-printing coats (thickness 28±7 μm, weight 6.07±0.72 mg cm^{-2}) sintering at 1,000 °C for 2 h shows lower polarization resistance of 0.183 Ω cm^2 at 800 °C. Based on the optimized parameters, the polarization resistances of the L58SCF–$Ce_{0.8}Gd_{0.2}O_{1.9-\delta}$ composite cathode display the R_p values of 0.067 Ω cm^2 at 800 °C, 0.106 Ω cm^2 at 750 °C, 0.225 Ω cm^2 at 700 °C, and 0.550 Ω cm^2 at 650 °C.

Keywords SOFC · Cathode · Impedance spectra · Fabrication

F. Qiang · K. Sun (✉) · N. Zhang · S. Le · J. Piao
Department of Applied Chemistry, Harbin Institute of Technology, Harbin 150001, China
e-mail: sunkn@hit.edu.cn

X. Zhu
Center for Post-Doctoral Studies of Civil Engineering, Harbin Institute of Technology, Harbin, Heilongjiang, 150001, China

Introduction

Solid oxide fuel cell (SOFC) is a device that converts the chemical energy of fuels directly to electricity through an electrochemical reaction of the fuels with an oxidant [1]. Recently, much attention has focused on lowering the operation temperature to intermediate temperatures (600~800 °C) in order to meet various application requirements, such as facilitating the use of cheap materials and improving the long-term stability. However, in the intermediate temperature range, the polarization resistance of cathode increases significantly and has become the main factor affecting the cell performance.

Three main approaches can be adopted to decrease the cathodic polarization resistance: (a) using mixed ionic–electronic conductor (MIEC) cathode materials [2]; (b) optimizing cathodic structure, such as selection of additives (binder and pore former), effect of coating thickness, sintering temperature and time; (c) adding an ionically conducting second phase such as yttria-stabilized zirconia (YSZ) or $Ce_{0.8}Gd_{0.2}O_{1.9-\delta}$ (GDC) to form a composite cathode [3].

In order to obtain the optimized fabrication process and decrease the cathodic polarization resistance, fabrication parameters and electrochemical performance of cathode membranes were investigated in this study. Fabrication parameters include selection of additives (binder and pore former), effect of coating thickness, and sintering temperature and time on the microstructure. One of the major technical barriers for widespread commercialization of SOFCs is their high manufacturing costs [4]. Ethyl cellulose is the conventional binder used in $La_{1-x}Sr_xMnO_{3-\delta}$ (LSM) cathode slurry to screen printing on the YSZ pellet. However, polyvinyl butyral (PVB) is seldom served as binders for cathode slurry. There seems

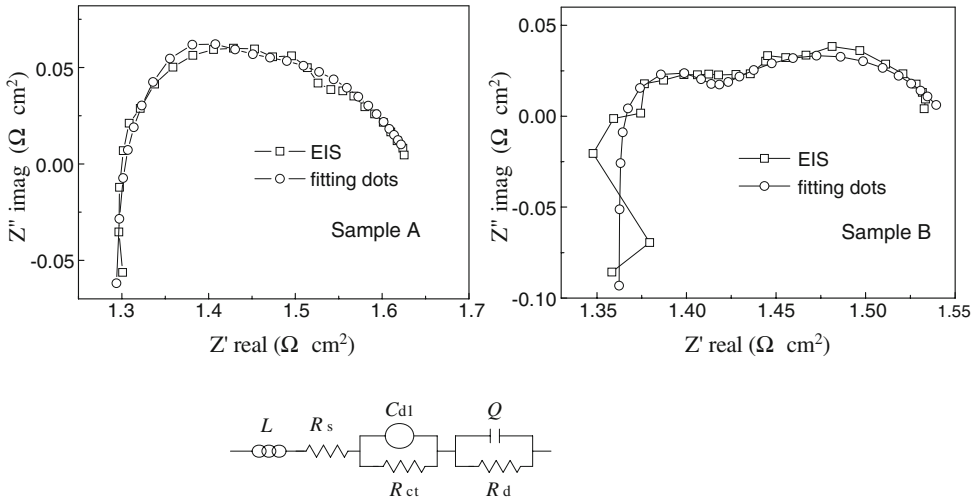

Fig. 1 The impedance spectra for the L58SCF cathodes sintered at 1,000 °C for 2 h and the equivalent circuit of impedance curves (ethyl cellulose as binder in *sample A* and PVB as binder in *sample B*)

to be no detailed study to date analyzing the feasibility of selecting the PVB as a binder for the $La_{0.58}Sr_{0.4}Co_{0.2}Fe_{0.8}O_{3-\delta}$ (L58SCF) cathode slurry. The manufacturing costs can be reduced by employing the inexpensive PVB binder. Organic material can be used as the pore former in the electrode because it can be burned out and leave residual porosity in the electrode body during the sintering process. Thus, the organic material PVB which served as pore former in the cathode can further reduce manufacturing costs, and it does not require other pore former additions. Furthermore, the proper thickness of cathode can also decrease polarization resistance because electrochemical reactions can take place throughout the thickness of the cathode [5]. However, the thickness needs to be confined below a certain thickness in order to avoid lower effective reaction sites and excessive concentration loss.

Electron–ion mixed conductor $La_{0.6}Sr_{0.4}Co_{0.2}Fe_{0.8}O_{3-\delta}$ (LSCF) possessing high conductivity in air at intermediate temperatures and high catalytic activity for the cathodic reaction is known to be one of the best alternatives compared to the LSM cathode material for intermediate temperature SOFCs [6]. A-site-deficient perovskite material L58SCF increases the ionic and electronic conductivity and the surface exchange of oxygen, due to larger number of oxygen vacancies and electronic holes in the L58SCF material [7]. In the previous study, we analyzed the MIEC composite cathode performance of addition of GDC to $La_{0.58}Sr_{0.4}Co_{0.2}Fe_{0.8}O_{3-\delta}$ [8]. In this study, the optimized process parameters on L58SCF cathode were used to fabricate the L58SCF–GDC composite cathode (60 wt.% L58SCF and 40 wt.% GDC). The electrochemical performance of L58SCF–GDC composite cathode was also investigated.

Experimental

GDC ($Ce_{0.8}Gd_{0.2}O_{1.9-\delta}$) powder was prepared by an oxalate coprecipitation route [8] with cerium nitrate hexahydrate ($Ce(NO_3)_3{\cdot}6H_2O$, 99.5%, Gansu Rare Earth Group) and gadolinium nitrate hexahydrate ($Gd(NO_3)_3{\cdot}6H_2O$, 99.5%, Gansu Rare Earth Group). L58SCF was synthesized by the citrate method [8] with these starting materials: La $(NO_3)_2{\cdot}6H_2O$ (99.5%, Gansu Rare Earth), $Sr(NO_3)_2$ (99.5%, Gansu Rare Earth), $Fe(NO_3)_3{\cdot}9H_2O$ (98.5%, Gansu Rare Earth), $Co(NO_3)_2{\cdot}6H_2O$ (99%, Gansu Rare Earth), and citric acid (99.5%, Tianjin Bodi).

YSZ powders (40 nm, Tosoh) were cold-pressed into pellets with the size of 13 mm in diameter and 0.7 mm in thickness and then sintered at 1,500 °C for 5 h. The average particle size of the starting powders was 0.47 μm (d50) for the L58SCF and 0.16 μm (d50) for the GDC by Laser Particle Sizer (LS900, OMEC). The slurry for the cathode was prepared by mixing L58SCF powder with the desired amount of pore former and binder in solvent (terpineol). The ratio of ceramic powder to terpineol is 1:2.96 (weight ratio). The slurry was then applied on one side of the

Table 1 The fitting components obtained by equivalent circuit of the impedance curves and the Rp of the cathode

	L (H cm^2)	R_s (Ω cm^2)	C_{dl} (F cm^{-2})	R_{ct} (Ω cm^2)	Q (Ω^{-1} cm^{-2} s^n)	N	R_d (Ω cm^2)	R_p (Ω cm^2)
Sample A	1.14×10^{-7}	1.28	0.0024	0.049	0.2470	0.4066	0.300	0.349
Sample B	1.51×10^{-7}	1.36	0.0011	0.045	0.6115	0.5716	0.138	0.183

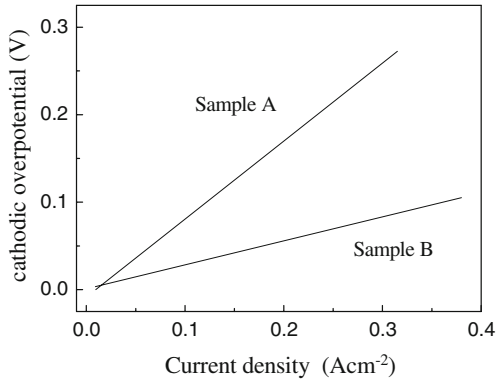

Fig. 2 DC polarization curves for the cathode tested at 800 °C. Ethyl cellulose as binder in *sample A* and PVB as binder in *sample B*

electrolyte by screen-printing method, which was followed by sintering at 1,000 °C for 2 h. The cathode area was about 0.25 cm^2.

In order to study the effect of different kinds of binders on the electrochemical performance of cathode, 4 wt.% ethyl cellulose and PVB were selected as the binders in the cathode slurry.

Carbon black and PVB were used as pore former, respectively, and 5 wt.% polyvinyl alcohol solution as binder. The L58SCF powders mixed with desired amount of pore former (0, 5, 10, and 20 wt.% of carbon black and 4, 8, 12, and 16 wt.% of PVB relative to the cathode powders) and binder were pressed at about 486 MPa to 25×5×3-mm flakes. The flakes were sintered at 1,000 °C for 2 h. The porosity of the sample was determined by Archimedes' method.

In order to analyze the electrochemical property of the cathode with carbon black as pore former, PVB was used as binder in the cathode slurry. While PVB was used as pore former, no other binder was added in the cathode slurry.

Morphology of the cathode was examined by a FEI SIRION scanning electron microscope (SEM). The element distribution was examined by energy-dispersive X-ray

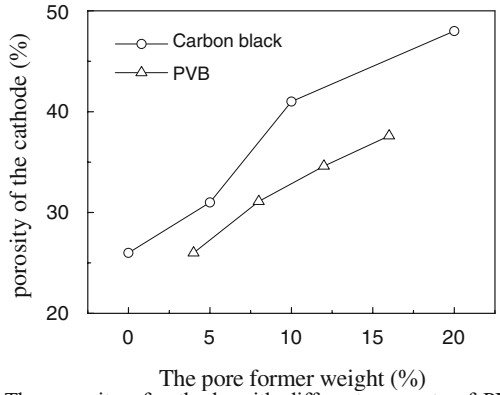

Fig. 3 The porosity of cathode with different amounts of PVB and carbon black pore formers

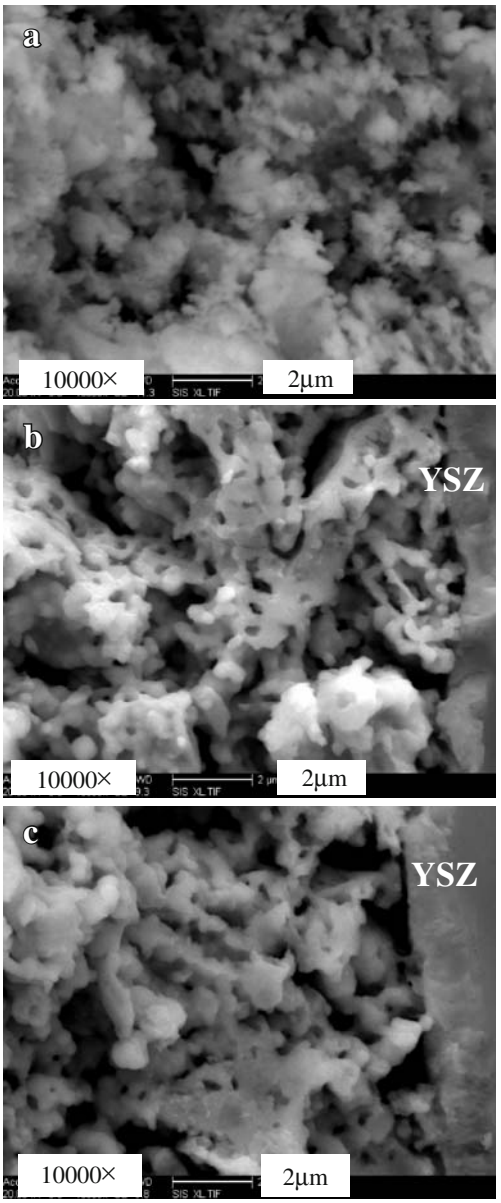

Fig. 4 SEM micrographs of cross section of cathode with carbon black pore former **a** 0 wt.%, **b** 10 wt.%, **c** 20 wt.% carbon black

spectroscopy (EDS, LeicaS440). The phase of L58SCF and L58SCF–GDC40 cathode was examined with Rigaku D/max-ΠB X-ray diffractometer (XRD) using Cu–Ka radiation. Impedance measurements were carried out using a potentiostat–galvanostat (model PARSTAT® 2273, Princeton Applied Research), with control and data collection handled by PowerSuite software. Three-electrode setup was used with the cathode as the working electrodes (WE). A commercial Pt paste (PC-Pt-7840, Sino-Platinum Metals) was applied to the edge of the same side of electrolyte as reference electrode (RE) and to the other side of electrolyte as the count electrode [8]. The frequency range was 10 mHz–10^5 Hz with a signal amplitude of 5 mV. The impedance fitting analysis was controlled with a software (Zsimpwin).

Table 2 The R_p and R_s of the cathode with PVB and carbon black pore former tested at 800 °C

	Carbon black			PVB	
	0%	10%	20%	4%	16%
R_p (Ω cm^2)	0.183	0.520	1.690	0.183	0.180
R_s (Ω cm^2)	1.360	2.180	2.580	1.360	1.250

Cyclic voltammetry measurements (scan rate 5 mV/s) between 0 and −0.3 V vs. the RE were performed using PARSTAT® 2273. Measurements were taken over a temperature range of 650–800 °C in air under open circuit potential.

Results and discussion

Selection of binder for screen-printing slurry

The selection of the binders can influence the microstructure and performance of the cathode membrane. The L58SCF cathode powders were made into slurry by being mixed with the binder (4 wt.% relative to the cathode powders) and organic solvent (terpineol) before screen printing. As the slurry binders for screen printing, ethyl cellulose and PVB were evaluated. Figure 1 shows the impedance spectra for the L58SCF cathodes sintered at 1,000 °C for 2 h and the equivalent circuit of the impedance curves to model the data (ethyl cellulose as binder in sample A and polyvinyl butyral as binder in sample B).

As shown in Fig. 1, the observed separable two impedance arcs at low and high frequencies for the L58SCF show that the oxygen reduction reaction is at least limited by two electrode processes during the molecular oxygen reduction. The oxygen reduction reaction had been modeled using a equivalent circuit, $LR_s(QR_d)(C_{dl}R_{ct})$, as seen in the Fig. 1 (resistance data obtained by impedance analysis at 800 °C); hereafter, all the impedance spectrum was fitted by the same equivalent circuit. The electrochemical impedance spectroscopy data were fitted to the equivalent circuit as shown in Table 1, with R_{ct}/C_{dl} and R_d/Q units in series with a resistor (R_s) and an inductor (L). The series resistance, R_s, corresponds to the overall ohmic resistance including the electrolyte resistance between the WE and the RE, the contact resistance at the electrode–electrolyte interface, and the resistance of the lead wires. The resistance R_d (on the low-frequency arc) may relate to the oxygen adsorption–desorption on the electrode particle surface and surface diffusion of intermediate oxygen species. The resistance R_{ct} (on the high-frequency arc) can be attributed to the charge transfer processes, which include oxide ion diffusion in the bulk of cathode and incorporation of oxygen ions from three-phase boundary (TPB) into YSZ lattice. The capacitance C_{dl}, as the double-layer capacitance, is contributed to the interfacial capacitance at the WE and YSZ electrolyte. Q is the constant phase element; n is

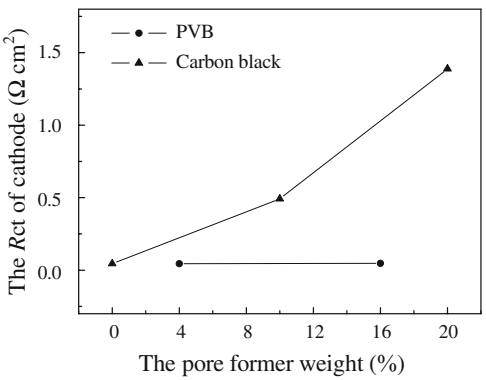

Fig. 5 The charge transfer resistances R_{ct} of the cathode with *carbon black* and *PVB* pore former, respectively

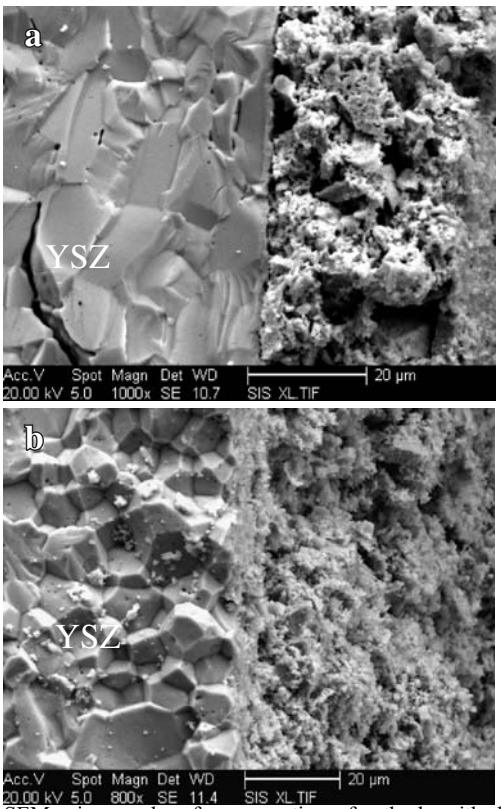

Fig. 6 SEM micrographs of cross section of cathode with different amount of PVB pore former **a** 4 wt.%, **b** 16 wt.% PVB

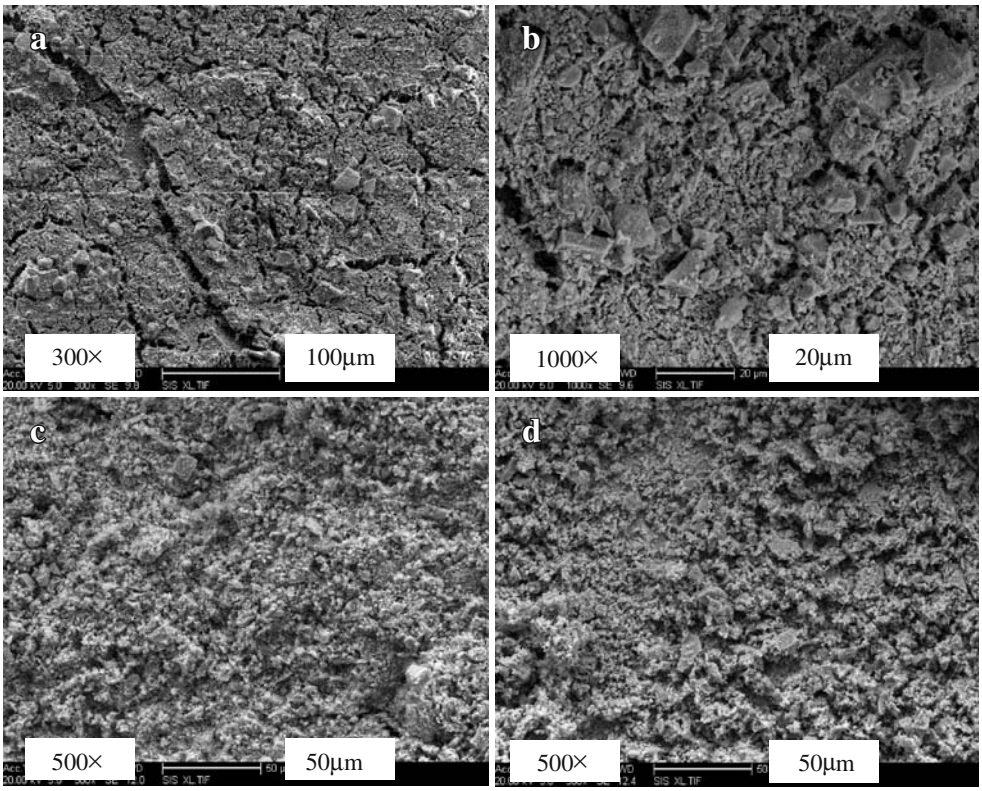

Fig. 7 SEM micrographs of cathode surface a with **a** 20% carbon black, **b** with 5% carbon black, **c** with 8% PVB, **d** with 16% PVB

the frequency power [9]. The cathode polarization resistance is composed of R_{ct} and R_d.

Though PVB has branches in its molecule structure, it dissolved easier into terpineol than linear polymer ethyl cellulose. When the cathode slurry was grinded, the long molecule chain of PVB dissolved in the slurry could be grinded and dispersed uniformly in the slurry. The cathode membranes in samples A and B adhered well to YSZ pellets. It was noted that the series resistance (R_s) of sample A is lower than that of sample B. In the experiment, the test conditions including electrolyte, the counter electrode, and reference electrode were identical; therefore, this phenomenon was a result of the fabrication error of YSZ pellets.

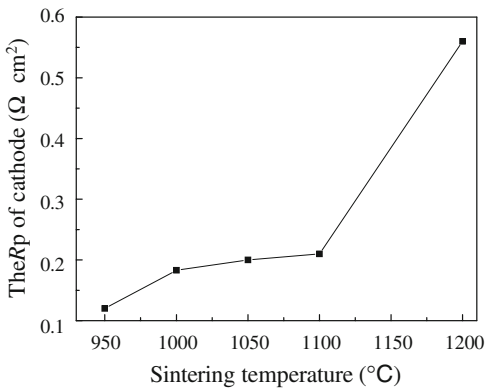

Fig. 8 The R_p of L58SCF cathode sintered at temperatures of 950, 1,000, 1,100, and 1,200 °C for 2 h

Table 1 shows that the R_{ct} of sample A (0.049 Ω cm^2) is approximately equal to that of sample B (0.045 Ω cm^2). The R_d of sample A was 0.30 Ω cm^2, while the R_d of sample B was 0.138 Ω cm^2. The sample of cathode membrane made by PVB possessed lower R_p than the sample made by ethyl cellulose as shown in Table 1. The decrease of R_p and R_d in sample B was due to the increase of TPB sites and higher porosity, respectively.

Cathode polarization curves of the L58SCF with different binders are shown in Fig. 2. The polarization current density of sample A is lower than that of sample B under the same overpotential condition. The result is in good agreement with that of impedance spectra. Thus, PVB is considered to be the preferable binder for L58SCF electrode to obtain uniform microstructures and high performance because of its good dissolvability in terpineol.

Selection of pore former material

The cathode should have sufficient porosity to allow gas transport to the reaction sites. Sufficient porosity and a fine-grained microstructure are desirable in the cathode close to the electrolyte–cathode interface to provide sufficient TPBs for the electrochemical reduction of the oxidant [4, 10].

PVB and carbon black, as pore-forming agents for the cathode, were evaluated. All the other processes and materials were maintained identical except for the pore

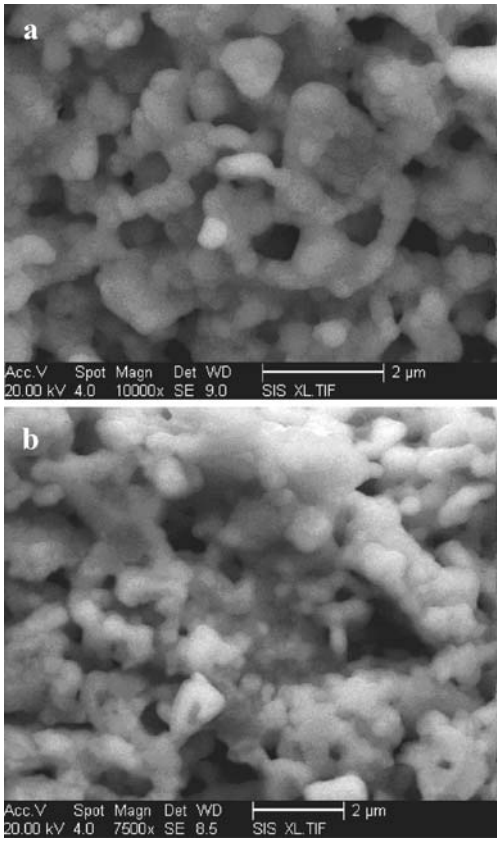

Fig. 9 SEM images for L58SCF cathode sintered at a 1,000 and b 1,200 °C

formers in the cathode; the cathodic thickness is between 21 and 35 μm. Carbon black was comprised of fine powders of amorphous carbon with a submicrometer particle size (0.3 μm), while PVB was a linear polymer dissolved easily in terpineol.

Ghosh et al. [11] indicated that the increase of open porosity was observed with increasing addition of the pore former in the LSM. A similar trend in the variation of open porosity was also observed for the samples with different amounts of pore formers, such as carbon black and PVB. In this study, 0, 5, 10, and 20 wt.% of carbon black and 4, 8, 12, and 16 wt.% of PVB relative to the cathode powders were chosen as pore former in the cathode, respectively. The amount of carbon black and PVB was also varied to increase the electrode porosity at the firing temperature of 1,000 °C. The porosity of sintered membranes with different amounts of carbon black and PVB were determined by Archimedes method. Figure 3 shows that residual porosity of the cathode increases with increasing amounts of pore formers; the porosity of the cathode with the carbon black (≥10 wt.%) is higher than that with the PVB (16 wt.%).

Figure 4 shows the cross-sectional SEM images of cathode with carbon black, after firing at 1,000 °C. With increasing of carbon black in the cathode, the porosity increases from 26% to 48%. The increase of the cathode porosity will improve gas diffusivity, but that also results in a lower solid volume fraction thereby reducing the effective electronic and ionic conductivity. With the addition of 20 wt.% pore former, 48% open porosity is obtained in the cathode. The membrane with 20 wt.% of carbon black was fragile and easily flaked off from the surface of YSZ pellet.

The effect of microstructural features on the electrode performance can be evaluated by an impedance spectroscopy. The polarization resistances (R_p) at 800 °C were compared for the cathode with different amounts of carbon black. The R_p values increase from 0.183 to 1.69 Ω cm^2 as carbon black in the cathode increases from 0 to 20 wt.%, as seen in Table 2. These observations can be explained by relating how porosity affected the effective ionic–electronic conductivities and the active reaction sites in the cathode. An increase in porosity results in facilitation of oxygen diffusion, which minimizes the oxygen transport limitation in the interface of electrode–electrode and/or electrode–electrolyte. However, the observed reduction in the R_p values with an increase in porosity could be attributed to the reduction in solid volume fraction, which results in less particle–particle contacts. Additionally, increasing porosity also causes reduction of effective electronic and ionic conductivity due to reduced solid fraction available for electron or ion transport [12]. As shown in Fig. 5, the R_{ct} of the cathode with carbon black are higher than that of the cathode with PVB. That indicates that higher porosity reduces the solid volume fraction and hampers the charge transfer in the electrode.

The cathode involving PVB pore former exhibits higher electrocatalytic activity toward the oxygen reduction as characterized by the lowest polarization resistance 0.183 Ω cm^2 (4 wt.% PVB) and 0.18 Ω cm^2 (16 wt.% PVB) at 800 °C (Table 2) as compared to the cathode with carbon black. These results are directly correlated with the microstructural features of the cathodes. Figure 6 shows that the cathode possesses sufficient fine pores and that particle–particle connects well in the cathode. The cathode with PVB pore

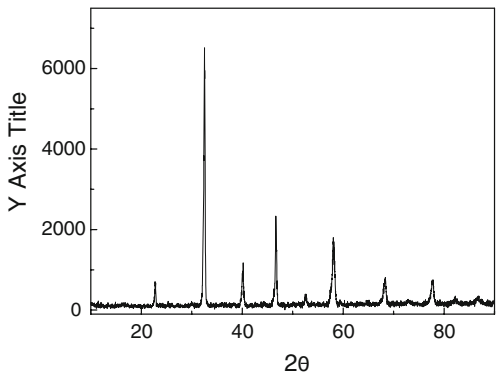

Fig. 10 XRD for L58SCF cathode on YSZ electrolyte sintered at 1,000 °C for 2 h

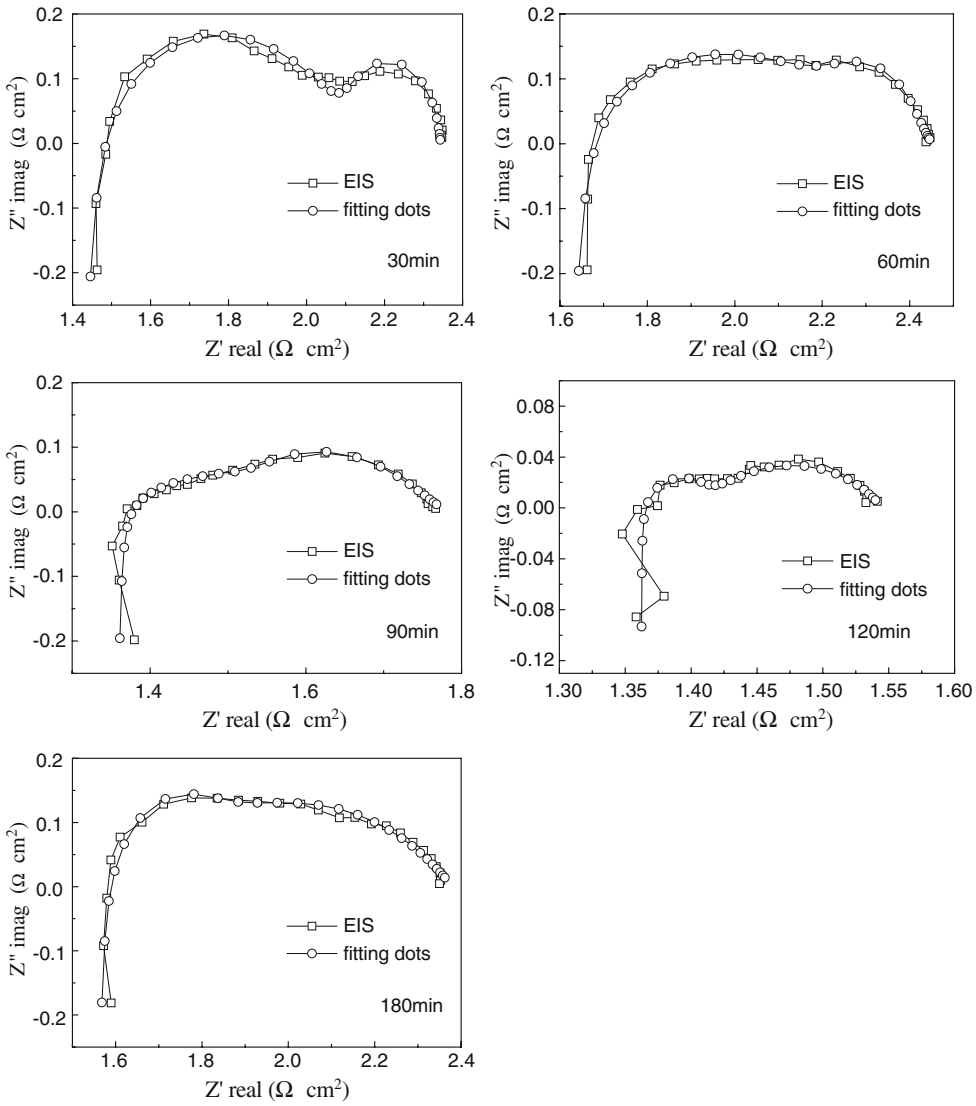

Fig. 11 Impedance spectra for the L58SCF cathode sintered at 1,000 °C for variety time

former in which sufficient porosity is present reveals higher cathodic performance. This improvement can be attributed to an increasing length of the triple-phase boundary in a porous electrode structure.

Yoon et al. [4] thought that carbon black was the preferable pore former due to its small particle size. But the cathode with carbon black pore former results a few small cracks, the cathode with PVB pore former being crack free (Fig. 7). The reason could be that increasing of cathode porosity also results in higher shrinkage of the cathode membrane during the sintering process. In addition, the cathode did not adhere well to the YSZ membrane due to the cracks in the cathode with carbon black. It induces that the R_s of the cathode with carbon black is higher than that of the cathode with PVB pore former (Table 2). Thus, the performance of the cathode was limited by the carbon back pore former [13].

Yan Ji et al. [14] indicated that the cathode should have the best performance when the porosity is in the range of 25~45%. In this study, the cathode with 26% porosity (PVB pore former) has better performance than that with more porosity (carbon black pore former). The reason could be because the pores uniformly and continually disperse in the cathode and promote the gas supply to the TPB and then substantially increase the gas penetration depth. Therefore, the availability of oxygen supply and reaction sites is confined to a very wide zone next to the gas–electrode interface.

Optimization of sintering processing parameters

It is found that these parameters [15], such as sintering temperature and sintering dwell time, have a large effect on the electrochemical property of cathode. These parameters

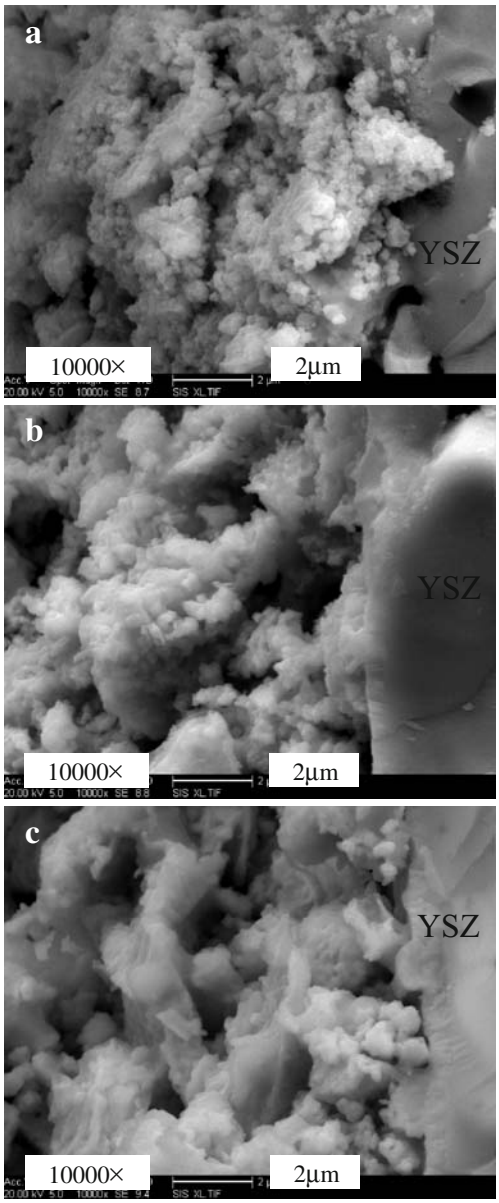

Fig. 12 SEM images of cross section for L58SCF cathode sintered at 1,000 °C for **a** 30 min, **b** 60 min, and **c** 90 min

are very effective on the membrane preparation. As a result, the effect of sintering temperature and sintering dwell time are studied as the most effective parameters on the performance of cathode.

Effect of sintering temperature

As already mentioned [15, 16], the sintering temperature has a pronounced effect on the microstructure of the cathodes and therefore influences the electrochemical performance of the cells. When optimizing the sintering temperature for a given electrode composition, the R_p of cathode must be taken into consideration. With respect to the R_p, the optimum sintering temperature can cause the maximum of the three-phase boundary length (TPBL) in the cathode membranes. Consequently, the R_p of L58SCF cathodes were sintered for 2 h at 950, 1,000, 1,050, 1,100, and 1,200 °C, respectively, and tested by electrochemical impedance spectroscopy (EIS) to obtain the optimum electrochemical performance. As can be seen in Fig. 8, the electrochemical performance is significantly lower after sintering at 1,100 °C than after 950 °C, which can be explained by the smaller intrinsic surface area of the cathode due to particle growth. The higher sintering temperature also increases formation of insulating phase such as $SrZrO_3$, which lowered the electrochemical performance of the cathodes [7].

The best performing sample in terms of EIS at 800 °C is the one sintered at 950 °C. However, the sample achieves inadequate adhesion among the particles in the cathode. Ag thread pasted on the cathode surface was easily flaked away from the cathode in the electrochemical experiment. Moreover, the sample sintered at 1,000 °C has adequate adhesion among the particles in the cathode, and its polarization resistance is 0.183 Ω cm^2 at 800 °C.

The microstructure of the electrodes is strongly affected by the sintering temperature [17], as illustrated in Fig. 9 for electrodes sintered at 1,000 and 1,200 °C. The density of the electrode increases with increasing sintering temperature. The increase of density is due to the decrease of the porosity and enhancing the grain size as shown in Fig. 9. The decrease in porosity may also directly affect the electrochemical property of the cathode.

Tu et al. [18] did not see a formation of additional phases between LSCF and YSZ at 800 °C after 96 h. The phases present in the cathodes, particularly the presence of any zirconate phases, were examined with XRD using Cu–Ka radiation [19]. No resistive phases $SrZrO_3$ were detected by X-ray diffraction for LSCF cathodes on YSZ sintered at 1,000 °C for 2 h (Fig. 10). The result is in good agreement with that of S.A. Barnett et al. [19]. When sintering temperature is increased, the reason of the depressed property of LSCF cathode should be that there may have some zirconate phase present at the LSCF–YSZ interface.

Moreover, if the sintering temperature is too high, the electrode microstructure becomes more coarse, which may lead to current constriction [20, 21].

Effect of sintering dwell time

Similar to the sintering temperature, the sintering time also has a significant influence on the electrochemical properties of the cathode. Figure 11 shows the impedance spectra for the L58SCF cathode sintered at 1,000 °C for various time. The size of the impedance arcs decreases with increasing sintering time from 30 to 120 min. When the sintering dwell time increases to 180 min, the impedance arcs

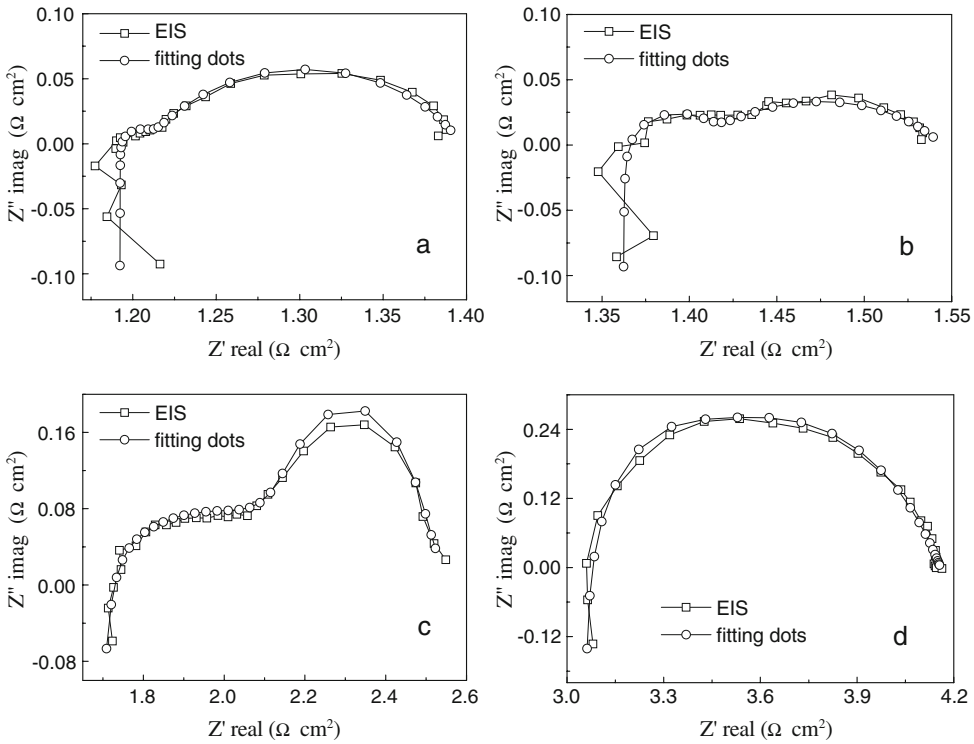

Fig. 13 Impedance spectra for the L58SCF cathode with **a** two coats, **b** three coats, **c** five coats, and **d** seven coats sintered at 1,000 °C for 2 h

increase. When the sintering time is 120 min, the impedance arc becomes smaller than other cathode arcs.

D. Weller et al. [22] reported that the LSCF electrode with the short sintering time (12 min) had both the lowest electrode resistance and activation energy. In our study, the L58SCF electrode sintered for 120 min had the lowest R_p than other sintering time. With increasing sintering time from 30 to 120 min for the L58SCF, the sizes of high-frequency arc are reduced gradually. It shows that extending sintering time can improve the charge transfer in the cathode. This phenomenon indicates the formation of necks (necks are formed by diffusion between adjacent, touching particles) among the particles playing a decisive role in enhancing the electrochemical kinetics of cathode [23]. Figure 12 shows that the particles of cathode are joined to one another with increasing sintering time. Figure 6a shows the SEM micrograph of the L58SCF cathode sintered for 120 min. The particles of L58SCF are found to be continuous and to form the three-dimensional framework in the electrode. The particles of the L58SCF are well attached to each other and a large number of pores in the membranes provide the gas a pathway to transport easily.

However, with increasing the sintering time, the grains agglomerate and grow; the number of the open pores reduces. It may degrade the electrochemical property for a longer sintering time. It shows that the best sintering dwell time is about 120 min and there is no need for longer time [15].

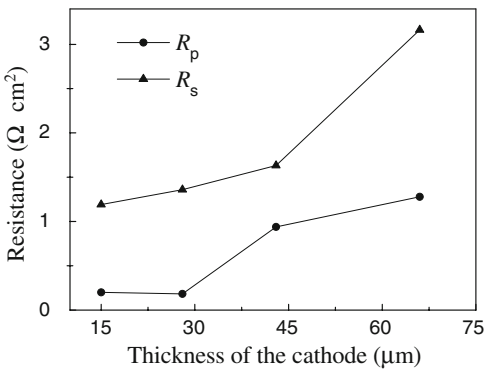

Fig. 14 The polarization resistances (R_p) and serial resistances (R_s) of L58SCF cathode as a function of the cathode thickness

Effective thickness of the cathode

To investigate the effective thickness, the cells with different electrode thickness were prepared, and the R_p and R_s were measured [24]. To increase the cathode membrane thickness, multilayer was coated onto the YSZ substrate.

The impedance spectra of the cathodes with thicknesses of 15±7~66±7 μm are plotted in Fig. 13. The thickness of the cathode should be taken into account when interpreting the results in Fig. 14, as R_p and R_s have previously been found to vary with increasing thickness [25, 26].

It can be seen in Table 3 that the R_{ct} of the cathode with five coats (0.2823 Ω cm^2) is over six times larger than that with three coats (0.045 Ω cm^2), and R_d of the cathode with five coats (0.6638 Ω cm^2) is nearly five times larger than that with three coats (0.138 Ω cm^2). The R_{ct} and R_d of the cathode with seven coats are larger than that with five

Table 3 Fitting results based on equivalent circuit of the impedance curves and the cathode weight on YSZ pellet for different cathode thickness

Cathode thickness)	Cathode weight (mg cm^{-2})	L (H cm^2)	R_s (Ω cm^2)	C_{dl} (F cm^{-2})	R_{ct} (Ω cm^2)	Q (Ω^{-1} cm^{-2} s^n)	N	R_d (Ω cm^2)
15±7 (2 coats)	3.14±0.82	1.49×10^{-7}	1.192	0.0111	0.017	0.7598	0.6981	0.1869
28±7 (3 coats)	6.07±0.72	1.51×10^{-7}	1.36	0.0011	0.045	0.6115	0.5716	0.138
43±7 (5 coats)	9.13±1.11	1.56×10^{-7}	1.632	0.9773	0.2823	0.2349	0.2858	0.6638
66±7 (7 coats)	12.19±1.5	3.02×10^{-7}	3.163	1.26×10^{-4}	0.313	0.0095	0.5526	0.976

coats. When the number of cathode coats is more than three coats, both R_d and R_{ct} are observed to increase significantly. This is explained by the fact that a further increase of the total effective length of the triple-phase boundary does not contribute to a higher performance due to longer diffusion path. The large thickness of cathode could hamper the gas diffusion and the current transfer in the electrode. The same variation of R_d between two coats and three coats can be interpreted that the lower locations of the oxygen adsorption–desorption in the electrode enlarge the R_d of the cathode with two coats. However, the R_{ct} of the cathode with two coats is lower than that with three coats. This result could be caused by the errors of the experiments.

Table 3 also shows that the polarization resistances of L58SCF cathode are improved by decreasing cathode weight from 12.19±1.5 to 6.07±0.72 mg cm^{-2}. However, decreasing the cathode weight to 3.14±0.82 mg cm^{-2} lessens the oxygen reduction reaction site in cathode. In addition, with the cathode weight increasing, the error of the cathode weight enhances from ±0.82 to ±1.5 mg cm^{-2}. The error of the cathode weight is caused by the screen-printing operation. In the future, we should optimize the process of screen printing to decrease further the error of the cathode weight.

As shown in Fig. 14, the R_s values do not change obviously when the coat thickness increases from 15±7 to 43±7 μm. But when the coat thickness increases to 66±7 μm, the R_s values obviously increase. The reason might be that, with increasing the cathode thickness, the cathode cannot adhere well to YSZ pellets due to the thermal expansion coefficient (TEC) distinction between L58SCF and YSZ. Therefore, the higher the contact resistance at the electrode–electrolyte interfaces the higher R_s values of cathodes.

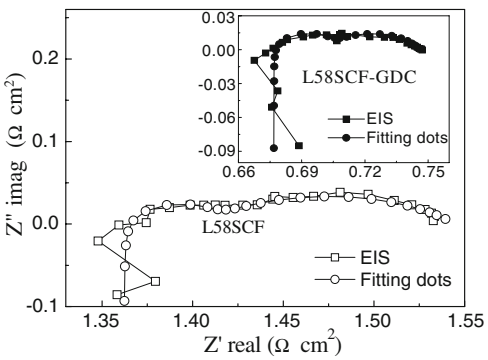

Fig. 15 Impedance spectra plots and the fitting curves for L58SCF cathode at 800 °C. *Inset* picture is for L58SCF–GDC composite cathode at 800 °C

The effective thickness of the electrode is 28±7 μm, as shown in Fig. 14, and it is consistent with the report of B. Kenney and K. Karan [12]. Yan Ji et al. [14] reported that when the composite cathode thickness was about 29.14 μm, the oxygen reduction reaction rate was the highest. Almost all active bonds of the cathode were used, no matter how far they were from the gas–cathode interface. However, when the thickness was increased beyond 30 μm, only the zone which was close to the electrolyte–cathode is well utilized for reaction. De Haart et al. [27] reported that the performance of cell did not depend much on the electrode thickness in the range of 5–10 μm [28]. This was explained by a limited percolation of ions and electrons when the thickness was less than 10 μm [26]. Haanappel et al. [29] studied the effect of LSM–YSZ cathode microstructure, functional layer thickness, and cathode current collector layer thickness and found that increased current collector layer thickness resulted in improved performance. Jiang et al. [30] studied the effect of interconnection coverage and found that increasing the interconnection coverage from 4% to 27% improved cathode performance. There had also been other studies showing the effect of functional layer thickness [31, 32]. A model by Virkar et al. [32] showed that the cell resistance of anode-supported cells was a function of the cathode thickness. The results in this study make it clear that the thickness (28±7 μm) of the cathode with three coats (cathode weight 6.07±0.72 mg cm^{-2}) could increase the cathode electrochemical property.

Performance of L58SCF–GDC composite cathode

The research of Hwang et al. [33] has indicated that the composite electrode adding GDC to the LSCF electrode resulted in a lower polarization resistance than the pure LSCF electrode. The composite cathode, the proper addition of the ionic phase GDC or samarium-doped ceria (SDC) to the cathode phase LSCF, results in the increase of TPB in the composite cathode and permits electrochemical reactions to occur within the electrode [19, 34]. In addition,

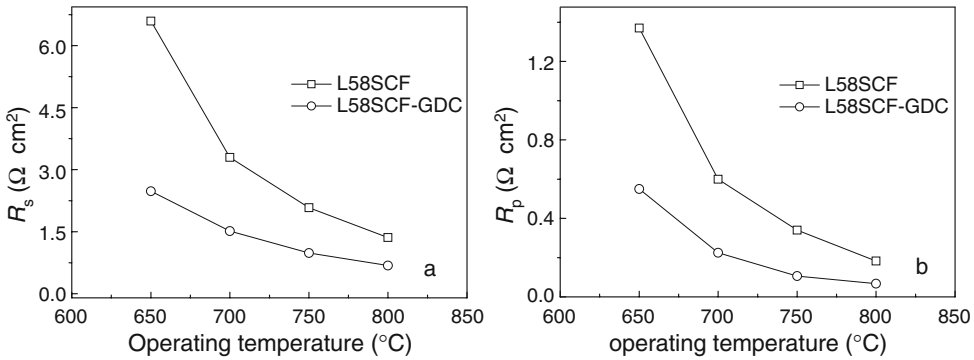

Fig. 16 The series resistance R_s (**a**) and polarization resistance R_p (**b**) for L58SCF–GDC composite cathode and L58SCF cathode

GDC in the cathode is considered to reduce the TEC without sacrificing the ionic conductivity. Thus, the optimized process parameters discussed above (PVB as binder and pore former, screen printing three coats, sintered at 1,000 °C for 2 h) were used to fabricate the L58SCF–GDC composite cathode (60 wt.% LS58CF and 40 wt.% GDC). The electrochemical performance of L58SCF–GDC composite cathode was also investigated.

Impedance spectra and fitting curves for L58SCF–GDC and L58SCF cathode are shown in Fig. 15. The impedance spectra of a pure L58SCF cathode and L58SCF–GDC composite cathode at 800 °C exhibit two semicircles, which suggest that there are two rate-limiting steps in our study case. The R_s values of the L58SCF–GDC cathode are lower than that of L58SCF cathode at various temperatures (Fig. 16a). This indicates that the particles of the L58SCF–GDC are well attached to YSZ electrolyte when the composite cathode membrane sintered at 1,000 °C for 2 h. The R_p values of L58SCF–GDC cathode and L58SCF cathode decrease significantly with the temperature increasing, as shown in Fig. 16b. The L58SCF–GDC composite cathode displays the R_p values of 0.067 Ω cm^2 at 800 °C, 0.106 Ω cm^2 at 750 °C, 0.225 Ω cm^2 at 700 °C, and 0.55 Ω cm^2 at 650 °C. The L58SCF cathode displays higher R_p values than the L58SCF–GDC cathode at the same temperature (Fig. 16b). It is conceivable that the interfacial polarization of the cell decreases with adding GDC in L58SCF. Conversely, the GDC–YSZ interfaces at the LSCF–GDC–YSZ interface would provide an easy path for ionic transport that bypasses the LSCF–YSZ interfaces, thereby reducing R_p [19]. The catalytic activity toward the reduction of the oxygen is significantly improved as indicated by the diminished polarization resistances form 1.37 Ω cm^2 (L58SCF) to 0.55 Ω cm^2 (L58SCF–GDC) at 650 °C. Hence, it is conceivable that the polarization resistance of the optimized composite electrode is decreased by extending TPBL, which results in much lower overpotential toward oxygen reduction, and by increasing the oxygen diffusion upon addition of an ionic conducting phase (GDC); thus, the composite cathode permits electrochemical reactions to occur within the electrode [35].

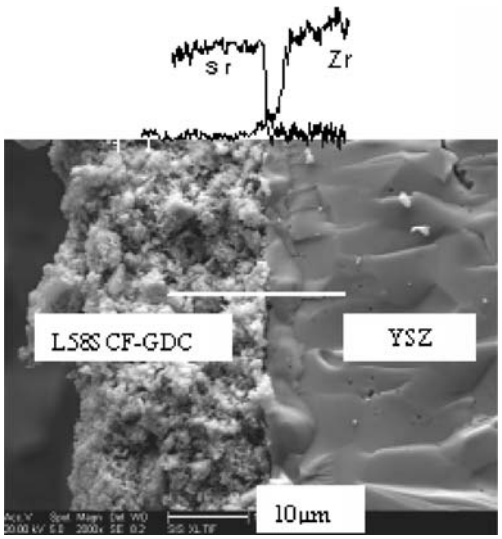

Fig. 17 EDS line scans for strontium and zirconium taken along the white lines of cathode with YSZ electrolytes. The baseline of the Sr and Zr lines are shifted for better readability. L58SCF–GDC sintered at 1,000 °C for 2 h on YSZ electrolyte

As can be seen in the EDS mappings in Fig. 17, the L58SCF–GDC cathode with YSZ showed no detectable SrZrO3 formation. The results show that the parameters of sintering temperature and time are suitable for the L58SCF–GDC composite cathode.

In the paper of W. G. Wang and M. Mogensen [36], the LSCF–GDC cathode was sintered at temperatures between 800 and 1,200 °C for 2–4 h. The measurement temperature range is from 500 to 800 °C. And aging experiment at 800 °C for the cathode of LSCF–GDC on YSZ electrolyte showed that no reaction products originated from a reaction between LSCF and YSZ. Thus, they thought that the LSCF cathode may be used directly on the YSZ electrolyte without cerium gadolinium oxide coating. Such SOFC system has to be operated well below 800 °C.

Xia et al. [37] prepared the LSM–GDC (50:50 wt.%) composite cathode via a sol–gel process and found the polarization resistance of the composite cathode was 0.28 Ω cm^2 at 700 °C. Murray and Barnett [38] reported that the R_p of the LSM–GDC50 on the electrolyte GDC was 0.34 Ω

cm^2 at 750 °C. Leng et al. [39] reported that the LSM–GDC composite (GDC 30 wt.%) cathode showed ≈13 times lower electrode polarization resistance (≈0.60 Ω cm^2 at 750 °C under open circuit) than that of pure LSM cathode (≈8.19 Ω cm^2 at 750 °C under open circuit) on YSZ electrolyte substrates. It is evident that the L58SCF–GDC composite cathode can be potential application on YSZ in intermediate temperature SOFC.

It is apparent that the optimized process parameters of fabricating cathode film are suitable not only for pure L58SCF cathode but also for the L58SCF–GDC composite cathode. According to the lower R_p of L58SCF–GDC composite cathode, it is a very strong cathode candidate for the low-intermediate-temperature SOFC.

In our next work, we will study endurance tests regarding the long-term electrochemical behavior of SOFCs with L58SCF-type cathodes and investigate the influence of barrier layer GDC on the degradation of the electrochemical performance.

Conclusions

The cathode membranes with PVB or ethyl cellulose binder adhere well to YSZ pellets. PVB is considered to be the preferable binder to obtain uniform microstructures and high performance for the L58SCF cathode.

Carbon black pore former can increase cathode porosity than PVB pore former; however, the high cathode porosity also results in higher shrinkage of the cathode layer during the sintering process. The cathode with carbon black caused small cracks, but the cathode with PVB was crack free. The electrochemical performance of the cathode is limited by the carbon black pore former. Thus, the PVB which is used as binder and pore former can reduce the manufacturing costs for SOFC.

With decreasing sintering temperature in the range from 1,200 to 950 °C, the electrode microstructure is found to be less dense and to contain smaller polarization resistance. The results show that sintering temperature of 1,000 °C and sintering dwell time of about 120 min are found to be the best temperature and the best time for sintering of the samples.

The large thickness of cathode can hamper the gas diffusion and the current transfer in the electrode. Additionally, the small thickness of cathode can reduce the current collecting ability in the electrode. The thickness (28±7 μm) of the cathode with three screen-printing coats can increase the cathode property.

The L58SCF–GDC cathode prepared by the optimized process parameters possesses better performance than L58SCF cathode. The L58SCF–GDC composite cathode displays the R_p values of 0.067 Ω cm^2 at 800 °C, 0.106 Ω cm^2 at 750 °C, 0.225 Ω cm^2 at 700 °C, and 0.55 Ω cm^2 at 650 °C. According to the lower R_p of L58SCF–GDC, it is a very strong cathode candidate for the low-intermediate-temperature SOFC.

Acknowledgements This project is financially supported by the National Natural Science Foundation of China (No. 90510006). The authors are very grateful for Prof. Phillip's careful checking of the paper and for Ph.D. Xiao Liang Zhou and workmate Shui Yun Shen's good discussions.

References

1. Song HS, Kim WH, Hyun SH, Moon J, Kim J, Lee HW (2007) J Power Sources 167:258
2. Wang ZC, Weng WJ, Chen K, Shen G, Du PY, Han GR (2008) J Power Sources 175:430
3. Murray EP, Tsai T, Barnett SA (1998) Solid State Ion 110:235
4. Yoon KJ, Huang WH, Ye GS, Gopalan S, Pal UB, Secombe DA Jr (2007) J Electrochem Soc 154(4):B389
5. Ni M, Leung MKH, Leung DYC (2007) J Power Sources 168:369
6. Lei Z, Zhu QS, Zhao L (2006) J Power Sources 161:1169
7. Mai A, Haanappel VAC, Uhlenbruck S, Tietz F, Stöver D (2005) Solid State Ion 176:1341
8. Fu Q, Sun KN, Zhang NQ, Zhu XD, Le SR, Zhou DR (2007) J Power Sources 168:338
9. Lee HK (2003) Mater Chem Phys 77:639
10. Tanner CW, Fung KZ, Virkar AB (1997) J Electrochem Soc 144:21
11. Ghosh A, Sahu AK, Gulnar AK, Suri AK (2005) Scripta Materialia 52:1305
12. Kenney B, Karan K (2007) Solid State Ionics 178:297
13. Song HS, Hyun SH, Moon J, Song RH (2005) J Power Sources 145:272
14. Ji Y, Yuan K, Chung JN (2007) J Power Sources 165:774
15. Mosadeghkhah A, Alaee MA, Mohammadi T (2007) Mater Des 28:1699
16. Jørgensen MJ, Primdahl S, Bagger C, Mogensen M (2001) Solid State Ion 139:1
17. Xu Q, Huang DP, Chen W, Lee JH, Kim BH, Wang H, Yuan RZ (2004) Ceram Int 30:429
18. Tu HY, Takeda Y, Imanishi N, Yamamoto O (1999) Solid State Ion 117:227
19. Murray EP, Sever MJ, Barnett SA (2002) Solid State Ion 148:27
20. Sasaki K, Wurth JP, Gschwend R, Godickemeier M, Gauckler LJ (1996) J Electrochem Soc 143:530
21. Hsu CH, Soong HT, Yu CC, Huang CL, Ku MT (2007) Ceram Int 33(6):951
22. Waller D, Lane JA, Kilner JA, Steele BCH (1996) Solid State Ion 86–88:767
23. Shojai F, Mäntylä TA (2001) J Mater Sci 36:3437
24. Fukunaga H, Ihara M, Sakaki K, Yamada K (1996) Solid State Ion86–881179
25. Carter S, Selcuk A, Chater RJ, Kajda J, Kilner JA, Steele BCH (1992) Solid State Ion 53:597
26. Juhi M, Primdahl S, Manon C, Mogensen M (1996) J Power Sources 61:173
27. Haart LGJ, Kuipers RA, Vries KJ, Burggraaf AJ (1991) J Electrochem Soc 138:1970
28. Ostergkd MJL, Mogensen M (1993) Electrochem Acta 38 (14):2015

29. Haanappel V, Mertens J, Rutenbeck D, Tropartz C, Herzhof W, Sebold D, Tietz F (2005) J Power Sources 141:216
30. Jiang S, Love J, Apateanu L (2003) Solid State Ion 160:15
31. Kenjo T, Osawa S, Fujikawa K (1991) J Electrochem Soc 138 (22):349
32. Virkar A, Chen J, Tanner C, Kim J (2000) Solid State Ion 131:189
33. Hwang HJ, Ji-Woong M, Seunghun L, Lee E (2005) J Power Sources 145:243
34. Adler SB (2004) Chem Rev 104:4791
35. Kenney B, Karan K (2007) Solid State Ion 178:297
36. Wang WG, Mogensen M (2005) Solid State Ion 176:457
37. Xia CR, Zhang YL, Liu ML (2003) Electrochem Solid State Lett 6:A290
38. Murray EP, Barnett SA (2001) Solid State Ion 143:265
39. Leng YJ, Chan SH, Khor KA, Jiang SP (2006) J Solid State Electrochem 10:339